Recent progress and future prospects with atmospheric neutrinos

2015 New J. Phys. 17 025006

(http://iopscience.iop.org/1367-2630/17/2/025006)

New Journal of Physics
The open access journal at the forefront of physics

Deutsche Physikalische Gesellschaft DPG
IOP Institute of Physics

Published in partnership with: Deutsche Physikalische Gesellschaft and the Institute of Physics

OPEN ACCESS

RECEIVED
14 August 2014

REVISED
8 December 2014

ACCEPTED FOR PUBLICATION
9 December 2014

PUBLISHED
13 February 2015

PAPER

Recent progress and future prospects with atmospheric neutrinos

Roger Wendell[1,3] **and Kimihiro Okumura**[2,3]

[1] Kamioka observatory, ICRR, University of Tokyo, Japan
[2] Research Center for Cosmic Neutrino, ICRR, University of Tokyo, Japan
[3] Kavli Institute for the Physics and Mathematics of the Universe, University of Tokyo, Japan

E-mail: raw@suketto.icrr.u-tokyo.ac.jp **and** okumura@icrr.u-tokyo.ac.jp

Keywords: atmospheric neutrinos, neutrino oscillations, atmospheric neutrino flux

Abstract

The large range of energies and pathlengths spanned by atmospheric neutrinos have made them a useful tool in the discovery and subsequent study of neutrino oscillations. With the recent measurement of the θ_{13} mixing angle, though it is now known that all mixing angles and mass differences in the PMNS oscillation framework are non-zero, several open questions, including the nature of the neutrino mass hierarchy, the value of the θ_{23} octant, and whether or not neutrinos violate charge-parity symmetry, remain. As atmospheric neutrinos are capable of addressing these issues as well as those from more exotic models, the importance of their continued role in neutrino physics is clear. Accordingly, this work reviews recent progress in the study of atmospheric neutrinos, including oscillation and flux measurements from ongoing experiments, and reports on future prospects for next-generation detectors.

1. Introduction

Though the neutrino is assumed massless in the standard model of elementary particles, the discovery of neutrinos oscillations using atmospheric neutrinos [1] and the subsequent observation of oscillations in solar, reactor, and beam neutrino experiments indicate that neutrinos are massive. Not only does this result highlight the incomplete nature of the standard model itself, but it has provided a point of access for theories seeking to address those deficiencies. For instance, potential explanations for the small but non-zero neutrino mass arise in several classes of models through the introduction of supersymmetry, extra dimensions, or heavy right-handed neutrinos [2, 3]. Each of these models addresses the relative lightness of the neutrino mass compared to that of the quarks and leptons through mechanisms not found in the standard model and frequently at scales relevant to grand unification. In this way the nature of the neutrino and its mass provide a unique window onto physics at energies not accessible through direct measurement.

Despite providing no information on the absolute scale of the neutrino masses, neutrino oscillations are nonetheless a sensitive probe of the differences between them. Not only has the existence of these oscillations been shown to resolve the reduced event rate observed in both atmospheric and solar neutrino measurements, but the precise values of the mass differences and the neutrino mixing angles can be used to constrain several classes of models predicting new physics [2]. Indeed, precision observations of neutrino oscillations can provide direct constraints on non-standard interactions with matter [4] and Lorentz invariance violating processes [5]. Additionally, the recent measurement of θ_{13} [6–8] has confirmed that all of mixing angles and mass splittings responsible for standard neutrino oscillations are non-zero [9]. With the subsequent observation of $\nu_\mu \rightarrow \nu_e$ oscillations [10] it has become possible to measure charge-parity (CP) symmetry violation in the lepton sector. For these reasons it is clear that neutrinos play an important role in searches for beyond the standard model physics.

Atmospheric neutrino observations are expected to make continued contributions in each of these areas. To that end the intent of this work is to review recent advances in the study of atmospheric neutrinos and comment on the relevance of future measurements. No attempt is made to detail the rich history of atmospheric neutrino studies and instead the present focus is restricted to measurements undertaken in the last five years. For a

thorough review of the early history of atmospheric neutrinos the interested reader is referred to [11]. The layout of this paper is as follows. Section 2 introduces the atmospheric neutrino flux and is followed by descriptions of general features of atmospheric neutrino interactions and their oscillations in sections 3 and 4. Starting in section 5 atmospheric neutrino measurements performed by current experiments are reviewed. Prospects for measurements using ongoing and future facilities are discussed in section 6 before summarizing in section 7.

2. Atmospheric neutrino flux

Produced from the decays of secondary particles emerging from the interactions of cosmic ray particles with air nuclei, atmospheric neutrinos represent a continuous source of neutrinos ranging in energy from $O(10^{-2})$ to $O(10^{6})$ GeV and above. Though the flux extends below 100 MeV [12], most atmospheric neutrino experiments are relatively insensitive to such low energy neutrinos and theoretical estimations of the flux are accordingly restricted to higher energies [13, 14]. Due to the isotropic nature of the primary cosmic ray flux, atmospheric neutrinos are produced across the Earth making it possible to observe neutrinos spanning a similarly broad range of pathlengths: from $O(10)$ to $O(10^{4})$ km. However, it is this combination of energy, E, and pathlength, L, which make these neutrinos particularly useful probes of the L/E structure of neutrino oscillations. At the same time the penetrating nature of the neutrino makes atmospheric neutrinos the dominant background in searches for proton decay, dark matter annihilation into neutrinos, and astrophysical neutrinos. A thorough characterization of the expected flux is therefore critical to measurements that consider atmospheric neutrinos as a signal or background source.

Indeed, deviations from this general picture become important for detailed studies of these neutrinos. It should be noted, for instance, that the flux of $O(1)$ GeV and lower atmospheric neutrinos exhibit a slight east–west anisotropy due the deflection of low energy primary cosmic rays in the earth's magnetic field [15]. Similarly, at $O(10)$ TeV and higher energies, the earth becomes opaque and interactions with its matter will attenuate the upward-going flux [16]. Incorporting these and other effects has become an important part of predicting the expected atmospheric neutrino flux at experimental cites.

Calculations of the atmospheric neutrino flux may be separated into 'conventional flux' and 'prompt flux' estimations, which are delineated based upon whether the neutrinos are produced from the decay chains of pions (π) and kaons (K) or charmed mesons emerging from the primary interaction, respectively. Due to the larger production cross section of pions and kaons, the conventional flux dominates the energy spectrum below ~100 TeV. As the interaction energy increases, however, the decay lengths of secondary hadrons increase, eventually becoming longer than their pathlength through the atmosphere. At this point the production of neutrinos from shorter-lived hadrons, predominantly D mesons, begins to dominate the spectrum. Due to the rapid decays of their parent hadrons, this prompt neutrino flux more closely follows that of the primary cosmic ray spectrum. Broadly speaking, the portion of the conventional flux below 100 GeV has yielded the most precise information on neutrino oscillations within the PMNS framework (presented in section 4) whereas the prompt flux represents an as-yet unmeasured background to searches for astrophysical neutrinos (see [19, 20]).

Modern flux computations perform detailed simulation and three-dimensional tracking of secondary hadrons and their decay chains, modeling the primary and subsequent interactions with standard hadron production codes. The effects of the earth's magnetic field, which enforces a rigidity cutoff for lower energy cosmic rays and bends the trajectories of charged secondaries, as well as the influence of the solar wind are included in these computations. Though the details of these calculations are beyond the scope of the present work, computations of the conventional and prompt fluxes are described in [14, 17, 21, 22] and [18, 23], respectively. It should be noted that while the absolute normalization of the expected flux is a sizable uncertainty common to these computations, the ratios of the flux components agree well among models, particularly below 50 GeV, and have considerably smaller uncertainties. The uncertainty in the absolute normalization ranges from ~20% to ~7% below 10 GeV, where uncertainties in both the pion production and interaction cross-section are significant, before rising again to roughly 25% at 1 TeV, where uncertainties in both the pion and kaon production cross section dominate [21]. On the other hand, below 100 GeV, the uncertainty in the ratios $(\nu_\mu + \bar{\nu}_\mu)/(\nu_e + \bar{\nu}_e)$, $\bar{\nu}_\mu/\nu_\mu$, and $\bar{\nu}_e/\nu_e$ are estimated to be within 2%, 5%, and 5%, respectively [21]. Example spectra from two flux calculations are presented in figure 1.

3. General features of atmospheric neutrinos

Cosmic ray muons represent the most serious background for atmospheric neutrino measurements. Since the interaction rate of atmospheric neutrinos (~100 kton^{-1} year^{-1} [24]) is much smaller than the vertical muon flux at sea level (~70 m^{-2} s^{-1} sr^{-1} [9]) atmospheric neutrino experiments must be performed underground. To differentiate downward-going cosmic ray muons from neutrino interactions within the detector experiments

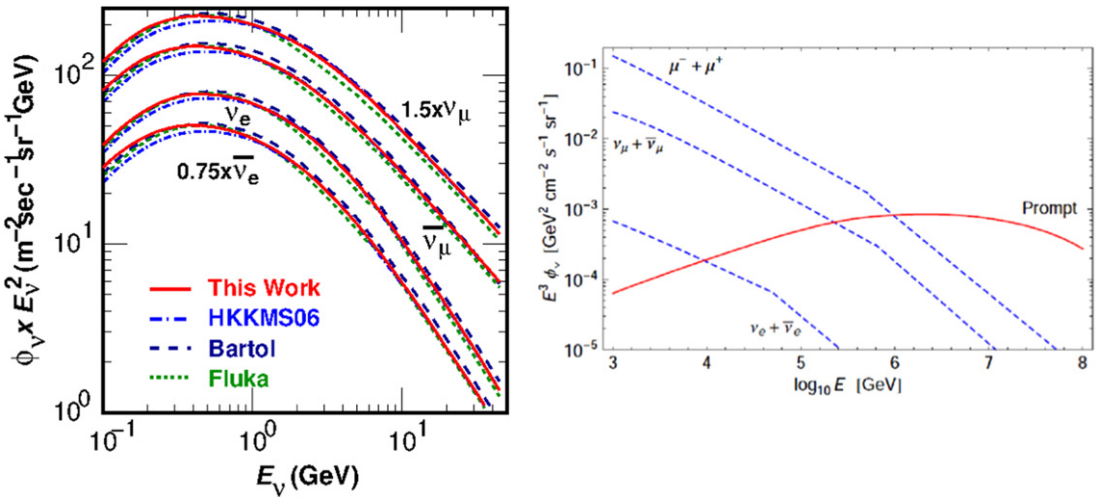

Figure 1. Calculations of the conventional and prompt atmospheric neutrino flux. In the left panel the calculation from [17] is compared with other similar computations. Reproduced with permission from Honda *et al* [17] . Copyright (2011) by the American Physical Society. The right panel shows the prompt (red) neutrino flux from [18] overlaid with estimations of the neutrino and muon flux from conventional computations. Reproduced with permission from Enberg *et al* [18]. Copyright (2008) by the American Physical Society.

often introduce an active veto or, in the case of extremely large detectors, use part of their active volume to tag entering particles. Unfortunately, it is not possible to distinguish cosmic ray muons from muons induced by neutrino interactions in the rock above an underground detector so both are removed from typical neutrino analysis.

Due to their variation in energy, atmospheric neutrino interactions include processes with single lepton final states induced by charged current quasielastic scattering (CCQE) processes as well as deep inelastic scattering (DIS) interactions with multiple particles escaping the initial interaction. This diversity produces several possible event topologies for detectors observing atmospheric neutrinos. At neutrino energies (E_ν) below roughly 1 GeV, the neutrino charged current interactions are dominated by the CCQE process, which for detectors incapable of identifying the hadron (proton or neutron) produced at the primary vertex manifests as a single lepton track ($e^\pm$, $\mu^\pm$). At intermediate energies, $1 < E_\nu < 10$ GeV, single meson production processes become increasingly relevant and create event topologies with multiple visible particles. Above this energy range DIS interactions dominate and interactions initiating within a detector are characterized by large hadronic energy deposition distributed among several particles. Since the true direction and initial energy of atmospheric neutrinos are unknown, the ability of a detector to contain the interaction products is essential for an accurate estimate of the parent neutrino properties. For all but the largest detectors, containing an $O(10)$ GeV muon leaving an interaction is often impossible or subject to acceptance limitations, so in many cases event topologies characterized by particles exiting the detector are utilized. Additionally, energetic muon tracks entering the detector at angles steep enough that the earth absorbs all cosmic ray muons are a signature of neutrino interactions in the surrounding rock. Such events are particularly useful in the study of atmospheric neutrino oscillations and were the mode of discovery for the first atmospheric neutrino experiments [25, 26].

The first observation of neutrino oscillations was characterized by a dearth of upward-going ν_μ-induced muon-like (μ-like) events in the atmospheric flux below $O(10)$ GeV. At the same time there was no evidence of distortions in the ν_e-induced electron-like (e-like) flux. For this reason the muon disappearance has been attributed to $\nu_\mu \rightarrow \nu_\tau$ oscillations, where the ν_τ often goes undetected due to the high production threshold of the τ; atmospheric neutrino oscillations are now known to be dominated by this mode [27, 28]. This phenomena can be illustrated using the muon neutrino survival probability assuming two-flavor mixing:

$$P(\nu_\mu \rightarrow \nu_\mu) = 1 - \sin^2 2\theta \sin^2\left(\frac{1.267\ \Delta m^2\left(\mathrm{eV}^2\right)\ \mathrm{L(km)}}{E_\nu\,(\mathrm{GeV})}\right), \quad (1)$$

where Δm^2 is the squared difference in the two neutrino masses, E_ν and L are the neutrino energy and flight length, respectively. For upward-going events, which must traverse part of the earth before detection, when $E_\nu <$ ~1 GeV the oscillation frequency in the second term becomes too fast to resolve experimentally and leads to an overall suppression of the flux in conjunction with the leading amplitude, $\sin^2 2\theta$, for $\Delta m^2 \sim O(10^{-3})$ eV^2. On the other hand, at very high energies this frequency becomes highly suppressed and no oscillation signal is seen.

The intermediate energy region then provides a sensitive probe of the mass splitting. It is worth mentioning that the lack of oscillations at high energies becomes an important feature not only in the characterization of the the high energy neutrino flux but also in the search for signals of exotic effects, such as those in Lorentz-violating models, which predict oscillation effects as a function of $L \times E$ [5]. A more detailed description of standard oscillations is presented in the following section.

4. Atmospheric neutrino oscillations

In the interest of completeness this section presents a brief review of the neutrino oscillation formalism in the context of atmospheric neutrinos. A more thorough description may be found in [9]. Though historically neutrino oscillations were often approximated using a two-neutrino framework, in light of recent measurements the following focuses on the three-neutrino scheme.

Oscillations arise in massive neutrinos due to mixing between the neutrino mass and flavor eigenstates. For three active neutrinos these may be written (ν_1, ν_2, ν_3) and $(\nu_e, \nu_\mu, \nu_\tau)$, respectively, and the correspondence between them is governed by a unitary mixing matrix, U

$$|\nu_\alpha\rangle = \sum_{i=1}^{3} U^{\star}_{\alpha,i} |\nu_i\rangle, \tag{2}$$

where Greek indices label the neutrino flavor. Known as the PMNS matrix [29, 30], this transformation may be parametrized by three mixing angles, θ_{ij}, and thereby decomposed as the product of three rotation matrices,

$$U = \begin{pmatrix} 1 & 0 & 0 \\ 0 & c_{23} & s_{23} \\ 0 & -s_{23} & c_{23} \end{pmatrix} \begin{pmatrix} c_{13} & 0 & s_{13} e^{-i\delta_{CP}} \\ 0 & 1 & 0 \\ -s_{13} e^{i\delta_{CP}} & 0 & c_{13} \end{pmatrix} \times \begin{pmatrix} c_{12} & s_{12} & 0 \\ -s_{12} & c_{12} & 0 \\ 0 & 0 & 1 \end{pmatrix}, \tag{3}$$

where c_{ij} (s_{ij}) indicates $\cos\theta_{ij}$ ($\sin\theta_{ij}$). In this scheme a CP violating parameter, δ_{CP}, is coupled to mixing in the 1-3 sector. The framework is completed by three mass differences, $\Delta m^2_{ij} \equiv m^2_i - m^2_j$, where m_i labels the mass of ν_i. Solving the Schrödinger equation in vacuum, the oscillation probability from one neutrino flavor, ν_α, into another, ν_β, becomes

$$P(\nu_\alpha \to \nu_\beta) = \delta_{\alpha\beta} - 4 \sum_{i>j} \Re\left\{ U^{\star}_{\alpha i}\, U_{\beta i} U_{\alpha j} U^{\star}_{\beta j} \right\} \sin^2\left(\frac{\Delta m^2_{ij} L}{4E_\nu} \right) + 2 \sum_{i>j} \Im\left\{ U^{\star}_{\alpha i}\, U_{\beta i} U_{\alpha j} U^{\star}_{\beta j} \right\} \sin\left(\frac{\Delta m^2_{ij} L}{2E_\nu} \right). \tag{4}$$

This equation illustrates the characteristic dependence of the oscillation parameter on the neutrino pathlengh, L, and its energy, E_ν. With the oscillation frequency determined by the mass difference of the neutrino states, Δm^2_{ij}, experiments can search for oscillations by choosing the ratio of these two quantities to maximize oscillations. It is this dependence that motivates atmospheric neutrino experiments to study their data as a function of reconstructed L/E.

Due to the appearance of only Δm^2_{ij} in equation (4) and not the individual masses, m_i, neutrino oscillations provide no information on the absolute scale of the neutrino mass. Further, the ordering of the neutrino masses cannot be determined using vacuum oscillations alone. At present the experimental data can be described equally well with two independent mass differences, $\Delta m^2_{21} \sim 7.6 \times 10^{-5}$ eV^2 and $|\Delta m^2_{32}| \sim 2.5 \times 10^{-3}$ eV^2, whose constituent masses are ordered in either of two scenarios. If the they are arranged in the order $m_1 < m_2 \ll m_3$ the mass hierarchy is referred to as 'normal' and if the ordering is instead $m_3 \ll m_1 < m_2$ it is referred to as 'inverted.' Whether the hierarchy is normal or inverted has important consequences for neutrinoless double-beta decay experiments as well as direct measurements of the neutrino's absolute mass (see [9]) and is connected to the ideas of grand unification [31, 32].

It should also be noted that the effects of the CP violating parameter, δ_{CP}, can only be realized if all of the other parameters in equation (3) are non-zero. Accordingly there is strong experimental motivation to measure each of them. Measuring them to a precision similar to that of the parameters describing quark mixing provides the most sensitive test of grand unified models [33] and is important for tests of the unitarity of the neutrino mixing matrix [34]. For instance, whether or not the value of θ_{23} is 45°, as modern data suggest, or slightly

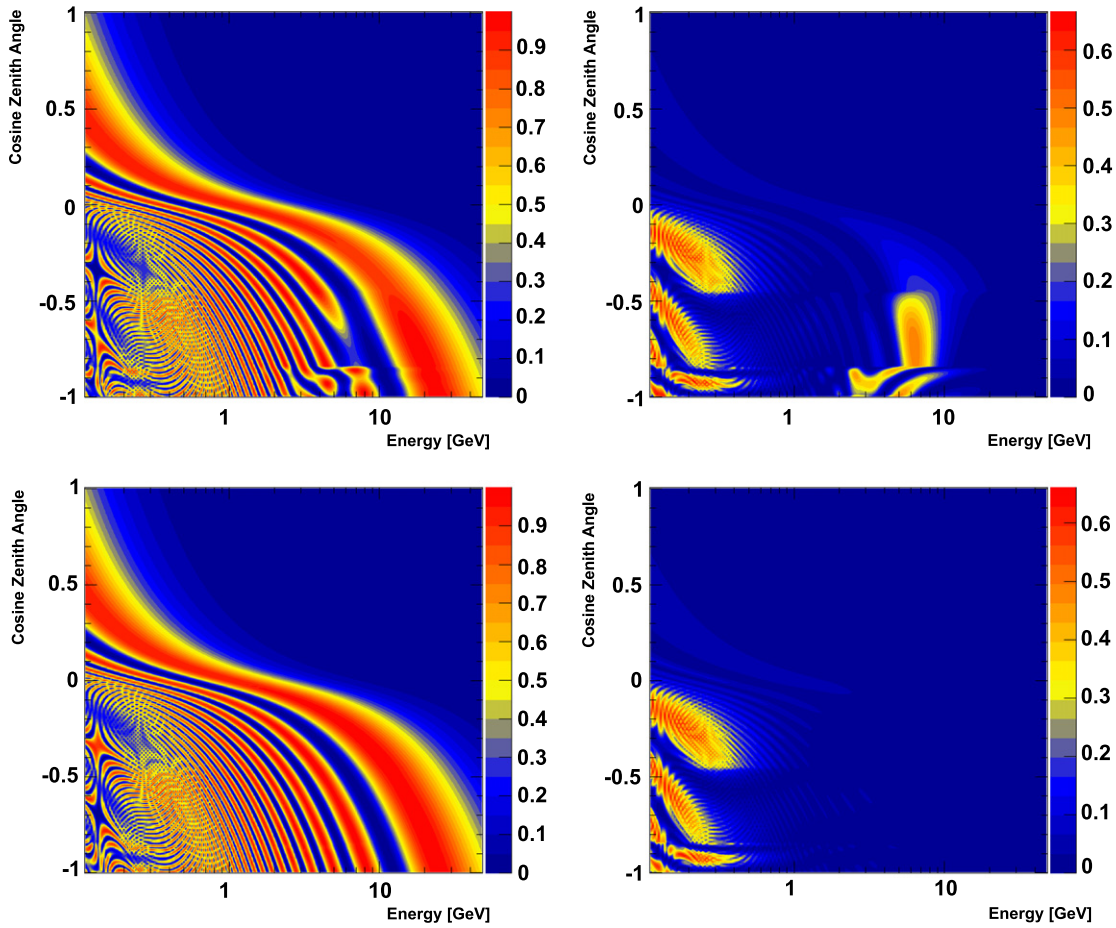

Figure 2. Neutrino oscillation probabilities as a function of zenith angle and energy. Cosine zenith of 1 (−1) indicates downward-going (upward-going) neutrinos. The left and right plots illustrate the $\nu_\mu \rightarrow \nu_\tau$ and $\nu_\mu \rightarrow \nu_e$ oscillation probabilities, respectively. The top and bottom rows show probabilities for the normal and inverted hierarchies, respectively. For antineutrinos (not shown) the figures are qualitatively similar, but resonance enhanced oscillations appear in the inverted hierarchy plots instead of the normal hierarchy plots.

different, falling into the first ($\theta_{23} < 45°$) or second ($\theta_{23} < 45°$) octant, would provide insight into the existence, or lack thereof, of additional symmetries in nature [35]. Fortunately, the effects of matter on neutrino oscillations can aid in both mixing parameter and mass hierarchy measurements.

For atmospheric neutrinos, which can traverse the diameter of the earth before interacting in the detector volume, the effects of matter cannot be ignored. Due to the presence of electrons in the planet's interior, charged current coherent forward scattering of ν_e on electrons gives rise to an effective potential in the neutrino evolution equation proportional to $V_e^{cc} = \pm\sqrt{2}\, G_F n_e$, where G_F is Fermi constant and n_e is the local electron number density. It should be noted that the potential reverses sign for antineutrinos. Though the three neutrino oscillation probabilities in arbitrary matter profiles cannot be described analytically, the problem has been solved for constant density matter [36]. Treating the earth's matter in piecewise steps of constant density (see [37]), the oscillations of atmospheric neutrinos can be completely characterized. Oscillation probabilities as a function of the cosine of the neutrino zenith angle, where −1 indicates the upward-going direction, and energy are shown in figure 2.

Several interesting features are present in the figure. Most notably, the non-zero nature of θ_{13}, $\sin^2\theta_{13} \sim 0.025$ [9] enhances the $\nu_\mu \rightarrow \nu_e$ oscillation probability for upward-going neutrinos when E_ν is between $2 \sim 10$ GeV. These features are characteristic of both MSW enhancement [38, 39] of the effective mixing angle in matter and of parametric resonances [40, 41], where the variation of the matter density along the neutrino trajectory correlates with changes in the oscillation phase. Due to the change in sign of the matter potential however, these resonant features are not present for antineutrinos when the mass hierarchy is normal ($\Delta m^2_{32} > 0$). This situation is reversed for an inverted mass hierarchy ($\Delta m^2_{32} < 0$), however, where only antineutrino oscillations are enhanced. Note that there is a distortion of the $\nu_\mu \rightarrow \nu_\tau$ oscillation probability in the same energy region. At energies below ~1 GeV oscillations are driven by the 1-2 mixing parameters. As these structures are sensitive to

the size of the atmospheric mixing angle, θ_{23}, δ_{CP}, and the sign of the mass hierarchy, atmospheric neutrinos are in principal sensitive to all of the current open questions in oscillation physics.

5. Current experiments

Due to the weak interactions of the neutrino and relatively low flux of the atmospheric neutrinos, large detectors are needed for precision measurements, particularly at energies where three-flavor oscillation effects are expected. To achieve this goal modern atmospheric neutrino experiments come in three generic detector types, water Cherenkov detectors, large volume ice or water Cherenkov telescopes, and iron tracking calorimeters. Water Cherenkov detectors, such as Super-Kamiokande, utilize an ultrapure water target contained within a large vessel. Its walls are lined with photosensors that observe Cherenkov radiation produced by charged particles emerging from neutrino interactions. Large volume ice (water) Cherenkov telescopes similarly utilize Cherenkov light to study atmospheric neutrinos, but generally instrument much larger volumes than traditional water Cherenkov detectors, using natural bodies of ice (water) to perform their measurements. Photosensors are placed along a three-dimensional lattice filling the target volume, which results in lower sensor densities and higher threshold energies. At present there are only two such telescopes, IceCube and ANTARES. Unlike these two technologies, iron tracker detectors, such as MINOS, are built from alternating planes of an active scintillator and iron layers to enable fine tracking of charged particles. The use of scintillator enables lower thresholds and magnetization of the iron layers provides charge sign selection and therefore separation of the ν and $\bar{\nu}$ flux. This section reviews recent results from each of these experiments. Results from previous experiments are reviewed elsewhere [11].

5.1. Measurements at Super-Kamiokande

Super-Kamiokande[42] is a cylindrical ring-imaging water Cherenkov detector measuring 39.2 m in diameter and 41 m in height. The detector is divided into an inner detector (ID) volume instrumented by 11 146 inward-facing 20 inch photomultiplier tubes (PMTs) providing a total photocathode coverage of 40%. Surrounding this volume and separated from the wall of the detector by 2 m is an outer detector (OD) that utilizes 1885 outward-facing 8 inch PMTs to veto environmental radiation and cosmic ray muons. A 22.5 kton fiducial volume is defined within the ID as the region offset from the ID PMT wall by 2 m. Between 1996 and 2013 Super-K has accumulated 4 220 days of atmospheric neutrino data corresponding to a 260 kton·year exposure.

Due to the large size of the detector and the variety of atmospheric neutrino energies, event topologies at Super-K fall into three categories based on the types of energy deposition in the inner and outer volumes. An event is considered fully contained (FC) if its primary vertex is contained within the fiducial volume and there is no energy deposition consistent with an exiting particle in the OD. Events with fiducial vertices but exiting tracks are classified as partially contained (PC). Muons produced by neutrino interactions in the rock surrounding the detector are identified as entering upward-going muon-like (μ-like) events and deposit energy in both the ID and OD. The upward-going muon and PC samples are further subdivided into stopping and through-going samples if the primary particle stops within the ID or OD respectively. FC events are further subdivided based on particle ID, electron (e-like) or μ-like, the number of visible Cherenkov rings, and the number of decay electrons. Particle identification is highly efficient and affords single-ring electron and muon misidentification probabilities of less than 1% [43].

To study atmospheric neutrino oscillations the data are divided into analysis samples according to figure 3 and each is binned in a zenith angle and energy variable. The dominant oscillation mode, $\nu_\mu \rightarrow \nu_\tau$, manifests as a deficit of muon-like events and is seen clearly in the figure, particularly for the upward-going bins of the multi-GeV and multi-ring samples. However, as outlined in section 4, the size of the mixing angle θ_{13} implies an enhancement of the $\nu_\mu \leftrightarrow \nu_e$ oscillation probability should be expected for multi-GeV neutrinos or antineutrinos depending upon the nature of the mass hierarchy. To take advantage of this asymmetry, the Super-K data are statistically separated into CC ν_e and $\bar{\nu}_e$ samples [45].

Fitting for oscillations in (Δm^2_{32}, $\sin^2\theta_{23}$, δ_{CP}) while treating $\sin^2\theta_{13}$ and the 1–2 parameters as nuisance parameters, yields the constraints shown in figure 4. Assuming either a normal or inverted hierarchy the Super-K data weakly favor atmospheric mixing in the second octant, $\sin^2\theta_{23} = 0.60$, but allow the first octant at approximately 1σ. A modest preference for the inverted hierarchy, at the level of 1.2σ is found in conjunction with a modest constraint on δ_{CP} [44]. The best fit value of Δm^2_{32} of 2.66×10^{-3} eV^2 and the size of the allowed region in the 2–3 mixing plane are consistent with the results from the T2K [46] and MINOS [47] measurements.

Due to the inconsistency of the Super-K data with the disappearance of the muon flux purely into unseen sterile neutrinos via $\nu_\mu \rightarrow \nu_s$ oscillations [48] and the preference of global data for oscillation into ν_τ, direct searches [28] for oscillation-induced ν_τ events are a critical component of verifying the standard mixing

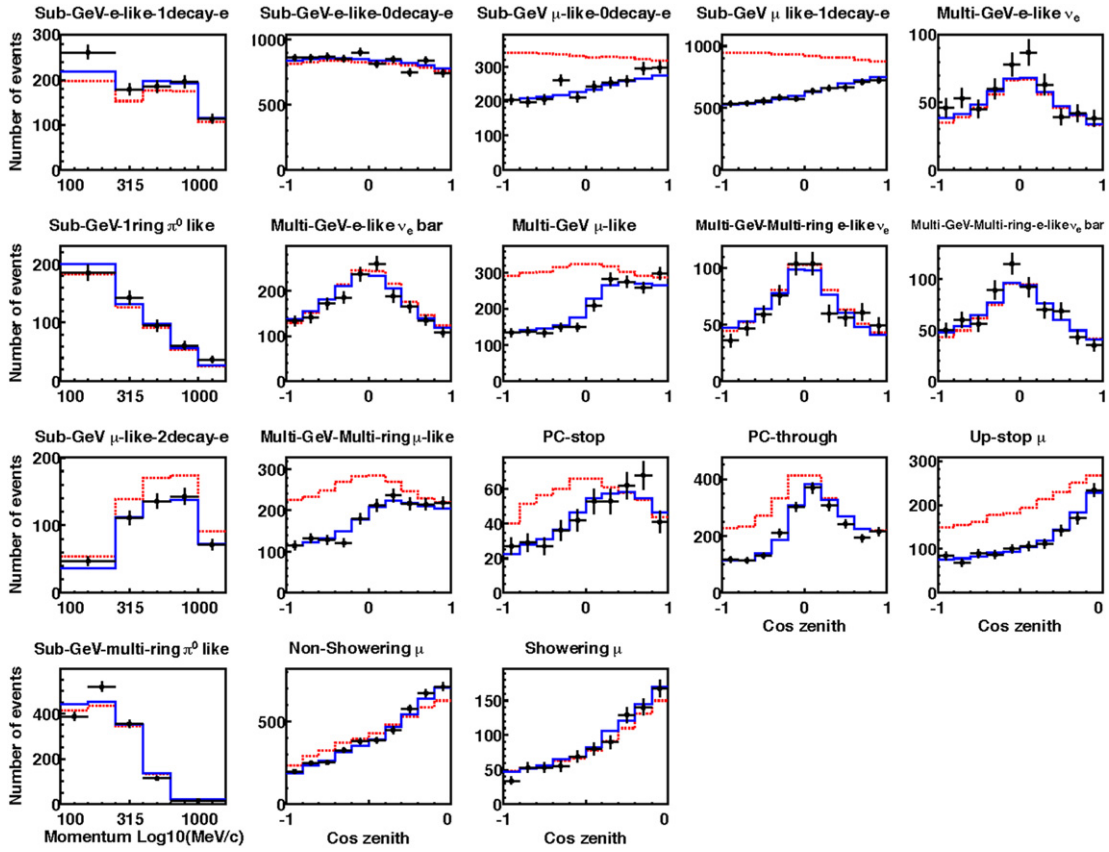

Figure 3. Super-K atmospheric neutrino zenith angle distributions from a 260 kiloton-year exposure of the detector. The Monte Carlo (MC) expectation assuming oscillations with $\sin^2\theta_{13} = 0.025$ is shown as the solid contour. The dashed line shows the unoscillated MC prediction [44].

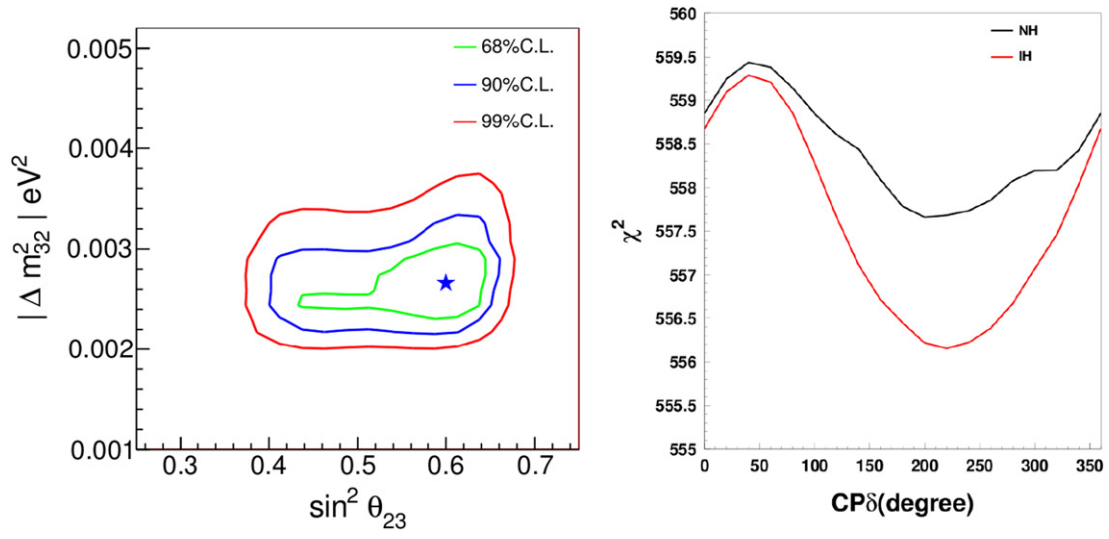

Figure 4. Results of the Super-K fit to three-neutrino oscillations. The left plot shows the $|\Delta m^2_{32}|$ versus $\sin^2\theta_{23}$ plane assuming an inverted mass hierarchy and a star indicates the best fit point. Constraints on δ_{CP} for fits to the normal and inverted hierarchies are shown in the right panel by the black and red lines, respectively [44]. The fit has 477 degrees of freedom.

paradigm. Assuming oscillations with $\Delta m^2_{32} = 2.4 \times 10^{-3}$ eV^2, the expected CC ν_τ interaction rate within Super-K is roughly $\sim$1 kton^{-1} yr^{-1} due to the 3.5 GeV production threshold of the τ. At Super-K the search for these events focuses on the hadronic decay modes of the τ lepton (branching ratio 65%) and employs a neural network technique for extracting the τ signal. Since the dominant ν_μ disappearance is seen in the upward-going data and there is no primary ν_τ flux below 100 GeV (cf figure 1), the signal is expected to appear only in the upward-going

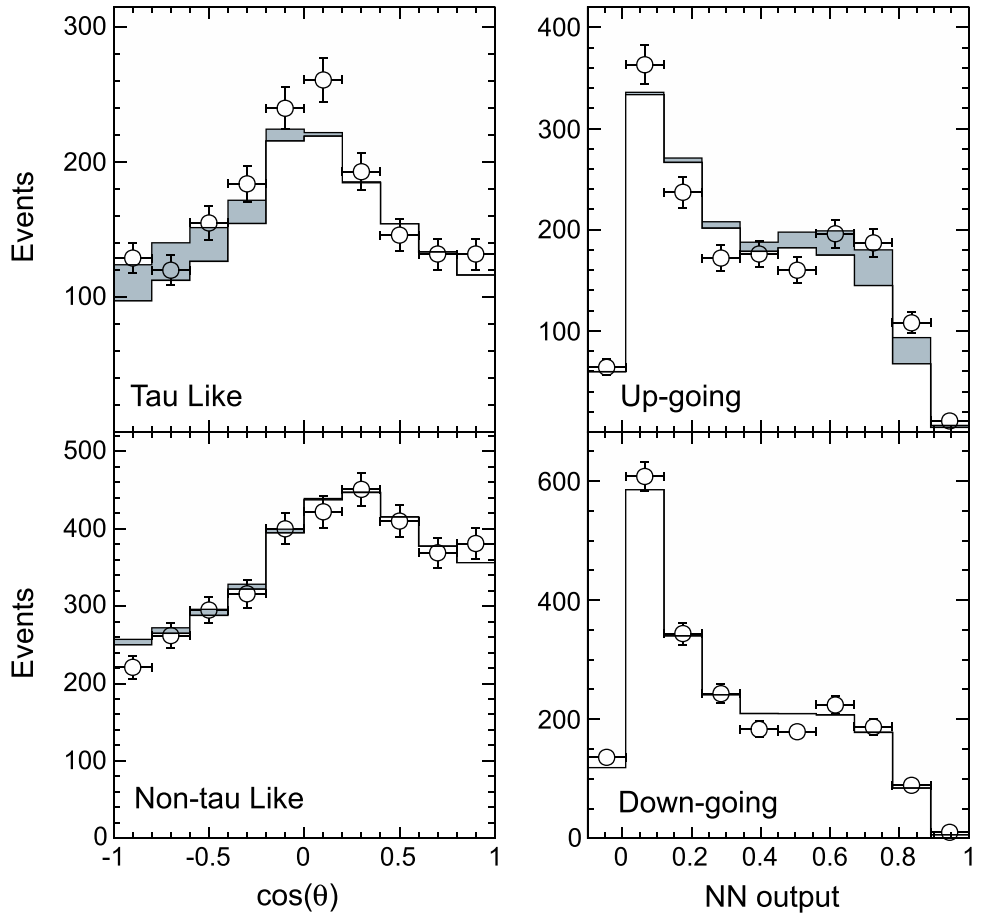

Figure 5. Cosine zenith angle (left) and neural network outputs from the Super-K search for oscillation-induced ν_τ events. The fitted ν_τ signal appears as the gray shaded histogram. Cutting at neural network output > 0.5 separates the τ-like events from the non-τ-like events [27]. Reprinted with permission from Abe *et al* [27]. Copyright (2013) by the American Physical Society.

electron-like data. After event selection and fitting, the number of observed events is $180.1 \pm 44.3(\text{stat})^{+17.8}_{-15.2}(\text{syst})$ compared to a base expectation of $120.2^{+34.2}_{-34.8}(\text{syst})$ [27]. The presence of the tau signal appears cleanly in the upward-going τ-like portion of figure 5 and provides 3.8σ evidence for the appearance of ν_τ from oscillations in the atmospheric data.

With the establishment of the PMNS mixing paradigm, deviations from these standard oscillations are an effective probe of beyond the standard model physics with atmospheric neutrinos. The possibility of additional non-standard neutrino interactions (NSI) can be parameterized generically as either flavor changing neutral current interactions (FCNC), where ν-fermion interactions alter the neutrino flavor, or as lepton universality-violating (NU) interactions which introduce different scattering amplitudes for each of the active neutrinos. A review of NSI and models that produce them is presented in [4]. Both types of interactions can be incorporated into the standard oscillation framework through the addition of an effective potential $\sqrt{2}\, G_f N_f V_{\text{NSI}}$, where G_f and N_f are the Fermi constant and local fermion number density, respectively. The diagonal (off-diagonal) matrix elements of V_{NSI}, $\epsilon_{\alpha\alpha}(\epsilon_{\alpha\beta})$ parametrize NU (FCNC) interactions. At Super-K the study of these interactions is divided into the μ-τ and e-τ sectors of the matrix, where the former distorts the $\nu_\mu \to \nu_\tau$ oscillations at $O(10)$ GeV, and the latter introduces effective oscillations between $\nu_\mu \leftrightarrow \nu_\tau \leftrightarrow \nu_e$ which alter the zenith distributions of the e-like and μ-like samples. Fits to both yield no indication of NSI. Constraints on $|\epsilon_{\mu\tau}| < 1.1 \times 10^{-2}$ and $-4.9 \times 10^{-2} < \epsilon_{\tau\tau} - \epsilon_{\mu\mu} < 4.9 \times 10^{-2}$ at 90% C.L. [49] have been obtained. Assuming $\epsilon_{\mu\tau}$ is represented equally by contributions from left-(L) and right-handed (R) fermions, $\epsilon_{\mu\tau} = \epsilon^L_{\mu\tau} + \epsilon^R_{\mu\tau}$, this result is compared to an accelerator-based measurement in figure 6. Constraints in the e-τ sector are dependent upon the assumed value of ϵ_{ee}, to which atmospheric neutrinos are insensitive. Assuming $\epsilon_{ee} = 0$ the 90% C.L. constraints become $\epsilon_{e\tau} < 0.024$ and $\epsilon_{\tau\tau} < 0.016$.

Though Super-K cannot generally distinguish neutrinos from antineutrinos on an event-by-event basis, the presence of both in the atmospheric neutrino data allows their separate oscillations to be studied statistically. Assuming the observed data are a combination of neutrino and antineutrino fluxes in proportion specified by the underlying flux model [21] and which oscillate independently of one another, Super-K has placed

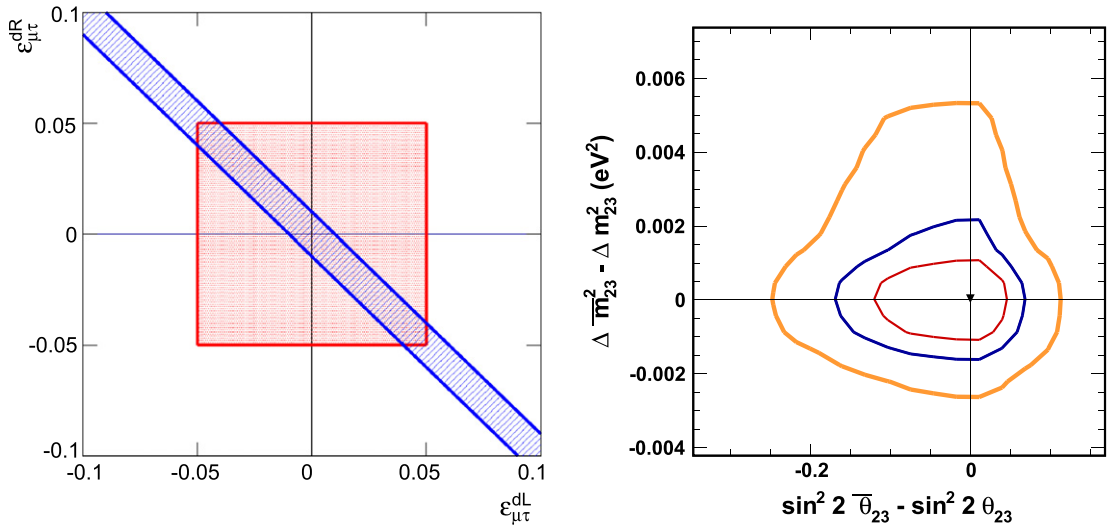

Figure 6. Constraints on NSI effects in the μ-τ sector (left). The blue region shows the Super-K atmospheric neutrino 90% C.L. result [49] and the red region is from [51]. Reprinted with permission from Mitsuka *et al* [49]. Copyright (2011) by the American Physical Society. Allowed differences between oscillation parameters at 68%, 90%, and 99% C.L. (in increasing size) assuming separate neutrino and antineutrino mixing from a fit to Super-K data [50] (right). Reprinted with permission from Abe *et al* [50]. Copyright (2011) by the American Physical Society.

constraints on antineutrino oscillations of the form $1.3 \times 10^{-3} \leqslant \Delta\bar{m}^2 \leqslant 4.0 \times 10^{-3}$ eV^2 and $0.83 \leqslant \sin^2 2\bar{\theta} \leqslant 1.0$ at 90% C.L. [50]. These oscillations are consistent with both the independent neutrino oscillation parameters and with Super-K's measurement assuming no difference between the species. The right panel of figure 6 shows the allowed differences between the neutrino and antineutrino oscillation parameters from this study.

It should be noted that since the proton's Cherenkov threshold is 1.07 GeV c^{-1} it is possible to reconstruct the those emerging from higher energy neutrino interactions. In practice, however, Super-K has demonstrated efficient reconstruction of protons with momentum $1.25 < p_p < 1.7$ GeV c^{-1}, due to the increased likelihood of creating light-producing particles through hadronic interactions at higher momenta [52]. Identifying a proton in conjunction with a charged lepton track enables the selection of a sample depleted in antineutrino interactions but with a neutrino purity of 91.7 $\pm$ 3% for which the parent neutrino's kinematics can be reconstructed. However, due to the narrow momentum range for reconstructing the proton and the reduced flux of neutrinos with energy sufficient to produce one, this sample suffers from low statistics. Only 78 μ-like and 47 e-like events were found in 2285 days of data. Despite this limitation an analysis of the reconstructed L/E distribution of these samples alone disfavors the 'no oscillation' hypothesis at the 3σ level [52]. This can be contrasted with the traditional SK L/E analysis [53], which selected 2726 events in 1489 days of data, and though lacking full kinematic reconstruction of the parent neutrino, constrains two flavor $\nu_\mu \leftrightarrow \nu_\tau$ mixing at the 90% C.L. to $1.9 \times 10^{-3} < \Delta m^2 < 3.0 \times 10^{-3}$ eV^2 and $\sin^2 2\theta > 0.90$ (cf equation 1).

5.2. MINOS measurements

MINOS [54] was designed to study neutrino oscillations using a beam of ν_μ produced at the Fermilab NuMI beamline and two magnetized-iron calorimeters: a near detector located ~1 km from the beam target and a far detector 735 km downstream. However, due to the 5.4 kton mass of the far detector and a 2070 m.w.e overburden the experiment also observes atmospheric neutrinos. Like other experiments, it is large enough to efficiently reconstruct both neutrino interactions originating within the detector and upward-going muons from interactions in the surrounding rock. However, unlike other recent experiments, the magnetization of the MINOS far detector enables sign selection of charged particles and can thereby distinguish neutrino and antineutrino interactions on an event-by-event basis.

The far detector is composed of planes of 486 vertically oriented steel plates interleaved with alternating planes of 1 cm thick scintillator strips aligned at $\pm 45°$ to the vertical. Each module has a height of 8 m and the collection of planes is divided into two supermodules 14.8 and 14.0 m in length and separated by 1.1 m. A toroidal magnetic field with an average field strength of 1.3 T is generated using a current loop that passes through a hole along the detector's axis and returns from beneath it. It should be noted that though the smaller near detector is functionally equivalent to the far detector, it is not used for atmospheric neutrino studies. A series of plastic scintillator modules has been placed above the detector in order to veto backgrounds from downward-going cosmic ray muons. Estimation of muon momenta is based on the fitted track length

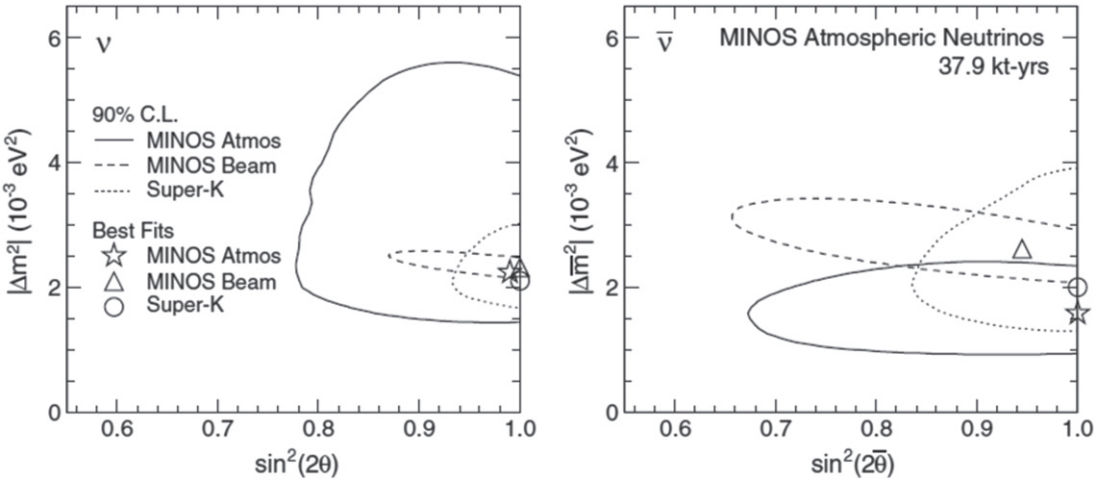

Figure 7. MINOS oscillation parameter constraints using atmospheric neutrinos. The left (right) panel shows the obtained 90% confidence level contours for a fit to the neutrino (antineutrino) data [55]. Additional contours from MINOS beam data and Super-K atmospheric data are shown for comparison. Reprinted with permission from Adamson *et al* [55]. Copyright (2012) by the American Physical Society.

(curvature) accounting for energy loss within the detector and curvature within its magnetic field for tracks which stop within (exit) the fiducial volume. In both cases the charge sign of the muon is based on the track curvature. While the Cherenkov threshold limits the ability of water Cherenkov detectors to observe hadronic activity near the neutrino interaction vertex, particularly low momentum particles, the granularity of its active layers and their low threshold for light production provide MINOS access to these particles. For interactions occurring within the detector MINOS can therefore make an improved estimate of the parent neutrino energy.

Between 2003 and 2011 MINOS accumulated 2553 live-days of atmospheric neutrino data corresponding to a 37.9 kton exposure. These data are divided for analysis into events with well reconstructed muon-like tracks and showering-like events produced by electromagnetic or hadronic particles. In the case of the latter, only a contained sample is used. The former, on the other hand, are divided into contained events and entering muons produced by neutrino interactions outside the detector. Each of these samples is further subdivided based on the charge sign of the muon candidate. This charge selection is 97% and 99% efficient for the contained and entering samples, respectively [55]. Forming a double ratio between the ratio of the number of upward- and downward-going events seen in the data and Monte Carlo (MC) prediction, $\mathcal{R}_{U/D} \equiv R^{\rm data}_{U/D}/R^{\rm MC}_{U/D}$, for a high resolution subset of the contained vertex sample yields $\mathcal{R}_{U/D} = 0.62 \pm 0.05(\text{stat}) \pm 0.02(\text{syst})$ assuming no oscillations in the MC. The deviation of this parameter from 1.0 is a $>6\sigma$ indication for oscillations [55]. A similar double ratio can be drawn from the charge-separated samples, $\mathcal{R}_{\bar{\nu}/\nu}$. For contained-vertex muons this ratio is measured to be $0.93 \pm 0.09(\text{stat}) \pm 0.09(\text{syst})$ and for entering muons it is $1.29^{+0.19}_{-0.17}(\text{stat}) \pm 0.16(\text{syst})$. Both measurements are consistent with unity, independent of the oscillation assumption. To study neutrino oscillations the data are binned in reconstructed L/E, where the neutrino pathlength is estimated based on the measured zenith angle of the muon. For contained vertex events the parent neutrino energy is based on the sum of the reconstructed muon and hadronic shower energies, whereas only the muon energy is available for the entering sample. In contrast to previous analyses studying the neutrino L/E distribution (see [53]), MINOS has adopted a method to maximize sensitivity to oscillations by further subdividing into four samples based on the expected L/E resolution [56]. Fits assuming two-neutrino oscillations as well as separate oscillation parameters for neutrinos and antineutrinos have been performed. The result of the latter is shown in figure 7. In both fits the MINOS atmospheric data are in good agreement with other measurements and no significant difference between the oscillations of neutrinos and antineutrinos is found. At the 90% C.L. the mass splitting difference between the two is constrained to be $|\Delta m^2| - |\Delta \bar{m}^2| = 0.6^{+2.4}_{-0.8} \times 10^{-3}$ eV^2 [55].

5.3. Atmospheric neutrinos at Sudbury Neutrino Observatory (SNO)

Though designed primarily for solar neutrino measurements, the SNO [57] has measured the atmospheric neutrino flux at 5890 m.w.e.. The SNO detector is housed in a 17.8 diameter steel geodesic vessel and separated into an inner 12 m diameter heavy water neutrino target and a surrounding 7.4 kton volume of ultra pure water by a 5.5 cm thick acrylic vessel. An array of 9456 20 cm PMTs lining the geodesic structure observe Cherenkov light in the inner volume of the detector. Due to the depth of the detector and its primarily flat overburden, SNO was able to study the slightly downward-going component of the neutrino flux using neutrino-induced muons

produced above the detector in addition to upward-going events. For all events passing the analysis selection cuts the total expected (observed) rate in the region $-1 \leqslant \cos\Theta_{\rm zenith} < 0.4$ is 138.4 (152) $\rm yr^{-1}$. The measured flux of neutrino-induced upward-going muon events, defined as $\cos\Theta_{\rm zenith} < 0$, was $2.10 \pm 0.12(\rm stat) \pm 0.08$ $(\rm syst) \times 10^{-13}$ $\rm cm^{-2}$ $\rm s^{-1}$ $\rm sr^{-1}$. Events with $0 < \cos\Theta_{\rm zenith} < 0.4$ had a measured flux of $3.31 \pm 0.23(\rm stat) \pm 0.13$ $(\rm syst) \times 10^{-13}$ $\rm cm^{-2}$ $\rm s^{-1}$ $\rm sr^{-1}$ [58]. When fit to a two-neutrino $\nu_\mu \rightarrow \nu_\tau$ oscillation model, the results are consistent with other atmospheric neutrino experiments and rule out the no oscillation hypothesis at the 3σ level. Utilizing constraints on the atmospheric mixing parameters from MINOS and Super-K, the atmospheric neutrino flux normalization is found to be consistent with the model from [14] and fits to 1.22 ± 0.09 [58] times its prediction.

5.4. IceCube/DeepCore

IceCube [59] is a neutrino telescope located near the South Pole that uses Cherenkov radiation in the Antarctic ice to observe charged particles. Though its primary objective is the detection of O(PeV) neutrinos from astrophysical sources, it observes atmospheric neutrinos down to much lower energies. The detector is composed of 86 vertical strings drilled into the ice and bearing 60 optical modules spaced at 17 m intervals along 1 km of cable. The optical modules (DOMs) are composed of 25 cm PMTs housed together with onboard digitization electronics in a pressure resistant vessel. IceCube's strings are separated by 125 m and instrument roughly a cubic kilometer of ice. However, the spacing of the DOMs determines the lower energy threshold: 50 ∼ 100 GeV [60]. To reduce this threshold to ∼20 GeV [61] and thereby enable the study of atmospheric neutrino oscillations, a more densely instrumented infill array, known as DeepCore [60], has been constructed. DeepCore uses 15 strings spaced at intervals between 42 and 72 m and achieves greater light collection than the base IceCube detector by using 50 DOMs per string, vertically separated by only 7 m, with each housing a high quantum efficiency PMT. The DeepCore array is located near the center of IceCube allowing it to use IceCube as an active veto for cosmic ray muon backgrounds.

Particle interactions at IceCube/DeepCore fall into two broad categories: tracks and cascades. The former are characteristic of high energy muons traversing the detector, produced from charged current ν_μ interactions in the surrounding environment or from cosmic ray muons. Showers, on the other hand, are more diffuse light sources and are generally created by the CC interactions of $\nu_{\rm e}$ or from NC interactions. It should be noted that there is no ability to distinguish CC ν from $\bar{\nu}$ interactions. Accordingly, IceCube has measured the atmospheric neutrino $\nu_\mu + \bar{\nu}_\mu$ energy spectrum using a zenith-averaged unfolding method on ∼18 000 upward-going track-like events in the energy range of 100 GeV to 400 TeV. The results are consistent with flux model of [21] in conjunction with any of a few models of the prompt neutrino flux [62]. In order to measure the $\nu_{\rm e} + \bar{\nu}_{\rm e}$ component of the spectrum, DeepCore was used. After selection cuts to remove cosmic ray muons and low energy muons from CC ν_μ interactions, the final analysis sample consists of 1029 events, half of which are estimated to be true cascade events. Subtracting off the background yields $496 \pm 66(\rm stat) \pm 88(\rm syst)$ cascade-like events and corresponds to a 4.5σ observation of the cascade signal. The resulting estimation of the $\nu_{\rm e}$ flux is consistent with conventional flux models [63].

In addition, IceCube/DeepCore has used a low energy sample of track-like interactions taken using eight of the DeepCore strings to study atmospheric neutrino oscillations [61]. In 318 days of data a sample of 719 muon-containing events with vertices within DeepCore was obtained. Assuming two-flavor oscillations these data indicate $|\Delta m^2_{32}| = (2.3^{+0.6}_{-0.5}) \times 10^{-3}$ $\rm eV^2$ and $\sin^2 2\theta_{23} > 0.93$ as shown in figure 8. This result is a detection of the oscillation signal with more than 5σ significance. Further, this result is consistent with measurements of both long-baseline experiments and Super-Kamiokande.

The IceCube atmospheric neutrino data have also been used to search for evidence of Lorentz invariance violation via a sidereal modulation of the event rate. Within the context of an effective field theory containing both the Standard Model Lagrangian and all terms that violate Lorentz invariance [64], the neutrino survival probability gains an intrinsic dependence upon the direction through which it propagates. Under these effects the neutrino interaction rate in the detector is expected to vary as a function of right ascension due to the rotation of the earth. Though no indication for such behavior is found in a 40-string subset of IceCube data, stringent limits on coefficients controlling Lorentz-invariance violation in this model have been established: $a_L^X,\ a_L^Y < 1.8 \times 10^{-23}$ GeV and $c_L^{TX},\ c_L^{TY} < 3.7 \times 10^{-27}$ at the 3σ confidence level [65].

5.5. ANTARES

ANTARES [66] is a neutrino telescope located deep in the Mediterranean which, like IceCube, has been designed to observe high energy neutrinos from non-terrestrial sources. The detector consists of 450 m 12 'lines' separated by 65 m from each other. Each line is equipped with 25 optical modules (storeys) separated by a vertical distance of 14.5 m. The Cherenkov light from upward-going muons produced by neutrino interactions in the sea water is detected by the storeys, allowing reconstruction of the muon direction. The parent neutrino energy is estimated from the pathlength of the observed muons.

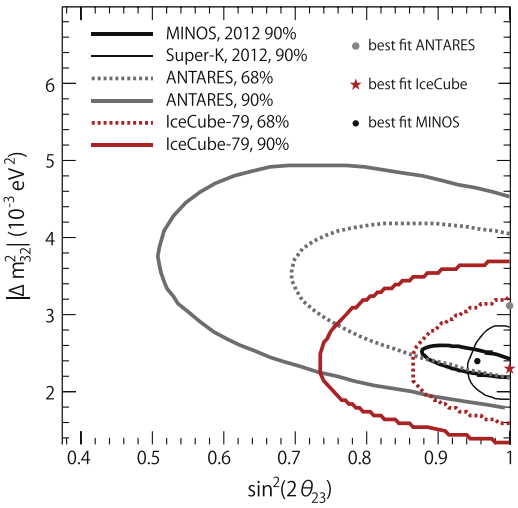

Figure 8. Allowed regions from the ANTARES and IceCube neutrino oscillation results compared with those of MINOS and Super-Kamiokande [61]. Reprinted with permission from Aartsen *et al* [61]. Copyright (2013) by the American Physical Society.

Due to the relatively large intervals between lines, the energy threshold for events to have hits across multiple lines is 50 GeV. Including single-line events, in which more than seven storeys have been hit, in the analysis lowers the energy threshold down to 20 GeV [67]. The reconstructed neutrino direction resolutions are estimated to be 0.8° and 3.0° for multi-line and single-line events, respectively.

After selecting events by the number of hit storeys, reconstructed direction, and fit quality, ANTARES has collected ~2000 events during 863 days of detector live time. Performing an oscillation analysis using the selected events yields $\sin^2 2\theta_{23}\,0 > 0.7$ with 68 % confidence level, and $\Delta m^2_{32} = (3.1 \pm 0.9) \times 10^{-3}$ eV^2 assuming $\sin^2 2\theta_{23} = 1.0$. The size of the obtained allowed regions is also shown in figure 8.

5.6. Systematic errors

Though many of the measurements presented in this section are in large part statistically limited, the effect of systematic uncertainties can nonetheless be important. In particular, systematic errors related to the atmospheric neutrino flux and the neutrino interaction model can have significant impacts, while detector systematics for current experiments have a lesser effect. Note, for instance, that the systematic error on the MINOS $\bar{\nu}/\nu$ double ratio measurements presented in section 5.2 have comparable sizes (~10%) to their statistical uncertainties due the relatively large error on the neutrino to antineutrino cross section ratio (8.5%) for the contained vertex sample and the 10% error on the high energy flux ratio for the entering muon sample [55]. Systematic uncertainties are often mitigated in oscillation parameter fits with the introduction of constraint samples. For the MINOS oscillation analysis, correlations between the neutrino and antineutrino samples help to constrain systematic errors on their flux and cross section parameters, leaving the absolute normalization of the samples as the only significant systematic effect on the oscillation parameter allowed regions [55]. The situation is similar for the IceCube/DeepCore measurement, where some systematics are moderated by including a non-oscillating high energy muon sample with the low energy oscillating sample in the fit. Though systematic errors affecting the shape of the muon zenith angle distribution, such as the atmospheric neutrino spectral index, are tightly constrained in this way, normalization uncertainties on the flux and the non-oscillating ν_e background component become significant [61].

Measurements at Super-Kamiokande are subject to similar limitations in the estimation of the atmospheric mixing parameters. However, the ability to simultaneously fit μ-like and e-like samples over a wide range of energies helps to constrain several aspects of the interaction and background model. Fitting both upward- and downward-going events places additional constraints on uncertainties in the flux model. As a result, measurements of the atmospheric mixing parameters at SK are mostly dominated by statistical and normalization uncertainties. This situation is compounded in the study of three-flavor effects, such as the mass hierarchy, due to both the reduced $\nu_e + \bar{\nu}_e$ flux at relevant energies and the increasing importance of systematic errors for the signal samples. Oscillation-induced ν_τ events, for example, populate a sizable portion of the upward-going electron-like data used to study the hierarchy. Accordingly, the 30% uncertainty on the CC ν_τ interaction cross section [68] can mask and therefore limit sensitivity to the hierarchy, particularly with larger data sets. Further, though Super-K attempts to divide its hierarchy-sensitive samples into neutrino-like and antineutrino-like components, poor purities and uncertainties in the selection [45] provide only weak

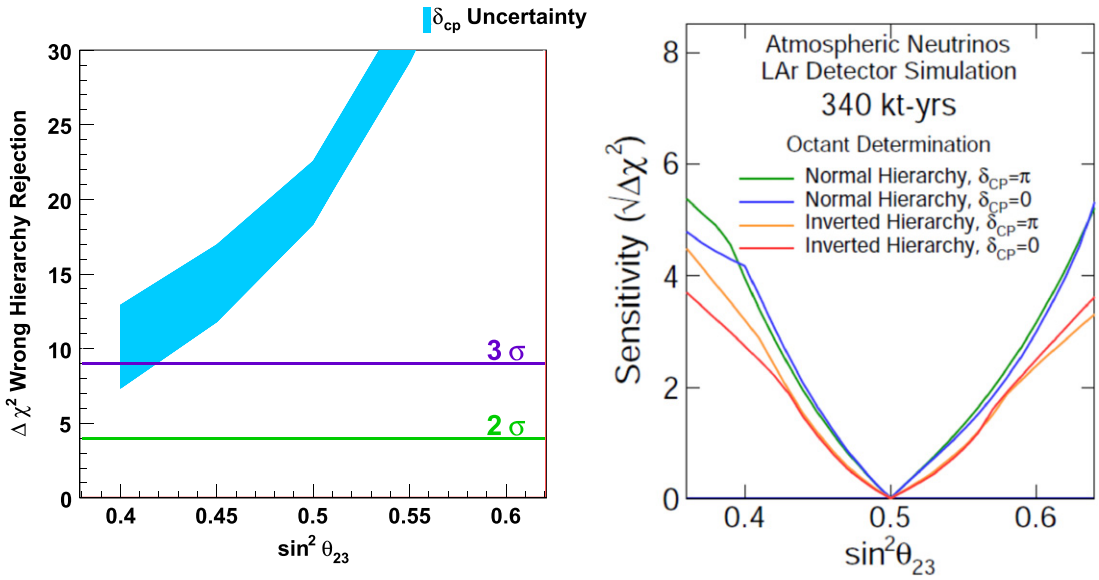

Figure 9. Atmospheric neutrino sensitivities for a ten year exposure of Hyper-K assuming the mass hierarchy is normal. The left figure shows the $\Delta\chi^2$ rejection of the wrong hierarchy hypothesis as a function of the assumed true value of $\sin^2\theta_{23}$. The uncertainty from δ_{CP} is represented by the thickness of the band [69]. Similarly, the right plot shows the ability to reject the wrong octant as a function of $\sin^2\theta_{23}$ for a 340 kton·year exposure of LBNE [70].

constraints on the $\bar{\nu}/\nu$ flux and cross section ratios, which impact the hierarchy sensitivity. Uncertainties relating to the pion production and interaction cross section are similarly important in the definition of signal samples with multiple Cherenkov rings.

Other analyses, such as the ν_τ appearance search presented in section 5.1, use only a subset of the atmospheric data sample and have lower ability to constrain flux and cross section uncertainties. Though the statistical uncertainty is roughly twice that of the systematic uncertainty for this analysis, half of the latter comes from the uncertainty in the ratio of the NC to CC cross sections [27]. Further, due to the large overlap of the ν_τ signal normalization and the effect of the uncertainty in the DIS cross section, which also affects the background in this analysis, the two were fit in parallel to limit the effect of the latter. Accordingly, despite the large statistical uncertainty in each of these measurements, improvements in the underlying flux and cross section models will be important for the next generation of experiments.

6. Prospects for future measurements

In both the short and long term, the most promising physics target in the future of atmospheric neutrinos is the measurement of the mass hierarchy. For current experiments a lack of statistics at multi-GeV energies, where hierarchy effects become most prominent, limits their sensitivity and suggests that larger detectors are necessary for a definitive measurement. Indeed, the measurement is possible using either ν_e appearance or ν_μ disappearance in atmospheric neutrinos and prospects for both at future facilities are presented briefly here.

6.1. Hyper-Kamiokande (HK)

HK is a proposed next-generation water Cherenkov detector designed to study neutrino CP violation using the J-PARC neutrino beam, nucleon decays, and atmospheric neutrinos. With a 560 kton fiducial volume it will accumulate atmospheric neutrinos at 25 times the rate of Super-Kamiokande and therefore offers unprecedented access to atmospheric neutrino physics.

Current sensitivity estimates are based on extrapolations of Super-K analyses to HK exposures assuming no additional improvements in the measurement or detector performance. Using 10 years of atmospheric neutrino data Hyper-K's expected sensitivity to the mass hierarchy exceeds 3σ for currently allowed values of θ_{23}, $0.45 < \sin^2\theta_{23} < 0.65$. The dependence of the sensitivity on the atmospheric mixing angle and its uncertainty due to δ_{CP} are shown in figure 9. Though not shown in the figure, the sensitivity does not depend significantly upon which hierarchy is true. If θ_{23} is non-maximal, Hyper-K can discriminate between the two θ_{23} octants at the 2σ level if $\sin^2 2\theta_{23} < 0.99$ [69]. Sensitivity to δ_{CP} using atmospheric neutrinos is suppressed both by its nature as a sub-dominant oscillation effect and by the uncertainties in the other oscillation parameters. As a result, only ~50% of

δ_{CP} space can be constrained at Hyper-K with atmospheric neutrinos and there is only weak sensitivity to CP-violation, sin $\delta_{CP} \neq 0$.

6.2. The Long Baseline Neutrino Experiment (LBNE)

Using a liquid argon based time projection chamber (TPC) the LBNE is a proposed experiment that, like HK, will observe both beam and atmospheric neutrinos. Though it is comparatively smaller at 34 kton, due to the low threshold of the TPC it is possible to reconstruct in fine detail the properties of both the lepton and recoiling hadronic system, which leads to improved resolution on the kinematics of the parent neutrino. This in turn gives LBNE unique sensitivity to neutrino interactions. For instance, while there are no plans to magnetize the detector, LBNE will be able to enhance its sensitivity to the mass hierarchy by statistically separating its atmospheric neutrino and antineutrino interactions via its particle identification capabilities. Protons, for instance, which are produced preferentially in CC neutrino interactions, are expected to be tagged with 100% efficiency when their kinetic energy is greater than 50 MeV.

LBNE's sensitivity to atmospheric neutrino oscillations has been estimated using a fast MC technique assuming 1° (10°) angular resolution for leptons (hadrons) and energy resolutions of 3%(15%) for contained (exiting) muons, $1/\sqrt{E}+1\%$ for electrons, and $30/\sqrt{E}\%$ for the hadronic system [70]. Binning in reconstructed zenith angle and energy and dividing the sample into FC electron-like and muon-like as well as PC interactions, LBNE is expected to achieve better than 3σ ($\equiv\sqrt{\Delta\chi^2}$) rejection of the wrong hierarchy with little dependence upon the value of δ_{CP} for a 340 kton·year exposure. Further, for $|\sin^2\theta_{23} - 0.5| > 0.05$ the θ_{23} octant can be determined at the 2σ level as shown in the right panel of figure 9. Much like the HK study, LBNE expects nominal sensitivity to sin $\delta_{CP} \neq 0$, reaching 2σ for only a handful of parameter scenarios.

6.3. ICAL at the India-based neutrino observatory

A dedicated atmospheric neutrino detector, ICAL, is being planned at the India-based neutrino observatory (INO). ICAL is a 50 kton magnetized iron calorimeter built from stacks of resistive plate chambers sandwiched between 6 cm thick iron plates. Though this configuration does not offer much sensitivity to the ν_e component of the flux, the application of a 1.5 T magnetic field allows for discrimination of $\mu^{\pm}$ and hence event-by-event neutrino and antineutrino tagging. With this separation, ICAL's sensitivity to the neutrino mass hierarchy is derived from the asymmetry of matter effects on neutrinos and antineutrinos passing through the Earth. Using an analysis of the L/E distribution of neutrino- and antineutrino-tagged events from a 1 Mton·year exposure, ICAL can make a $\sim 3\sigma$ determination of the mass hierarchy for $\sin^2 2\theta_{13} \sim 0.095$ [71] The sensitivity to the θ_{23} octant is expected to be $1(2)\sigma$ if $|\sin^2\theta_{23} - 0.5| > 0.05(0.10)$ Additionally, ICAL aims to constrain sterile neutrino mixing at $\Delta M^2_{\text{sterile}} \sim 1\ \text{eV}^2$ and to probe Lorentz violation.

6.4. PINGU and ORCA

Exploring the mass hierarchy using multi-megaton scale ice or water Cherenkov detectors with reduced thresholds (~1 GeV), such as the proposed upgrade of the IceCube detector, PINGU [72, 73], and that of ANTARES(KM3NeT), ORCA, has been discussed in [74]. Conceptually the two detectors are similar in that both utilize a denser infill array of optical sensors to lower their energy threshold down to $O(1)$ GeV levels and thereby gain access to earth-matter effects in atmospheric neutrino oscillations. Though these detectors are not well suited to observing isolated ν_e interactions, making use of the neutrino energy and zenith angle distribution of a high statistics sample of ν_μ events at these energies is sufficient to determine the mass hierarchy at 2σ via the disappearance channel alone. That being said, PINGU studies indicate that the sensitivity can be improved to 3σ with a few year exposure, by including cascade events in the analysis. Phenomenological studies have shown that the though the sensitivity may vary considerably depending upon the size of the assumed systematic uncertainties [74, 75], these can be mitigated by improved analysis techniques and the inclusion of cascade events [76]. Detailed studies considering more realistic detector performance and simulations have been performed by both experimental groups to determine the expected sensitivity under a variety of detector configuration and systematic error assumptions [72, 77].

7. Summary

Atmospheric neutrinos have been an essential part of both the discovery and study of neutrino oscillations. Indeed, there is now evidence for the appearance of ν_τ events in the atmospheric data, providing direct support for the $\nu_\mu \leftrightarrow \nu_\tau$ hypothesis as the explanation for the disappearance of the upward-going muon flux, and until only very recently atmospheric neutrinos provided the most stringent constraints on the mixing angle θ_{23}. Beyond the standard PMNS oscillation framework current experiments have also placed strong limits on exotic

models, including those with NSI, Lorentz invariance violation and CPT violating oscillations, further demonstrating the versatility of these neutrinos.

Yet there remain open issues, including the nature of the prompt atmospheric neutrino flux and the neutrino mass hierarchy, which these neutrinos can address. With the measurement of the last unknown mixing angle, θ_{13}, atmospheric neutrino data can be used to probe the mass hierarchy. Not only can this be done using the $\nu_\mu \rightarrow \nu_e$ appearance channel, but recent measurements with neutrino telescopes have achieved thresholds low enough to observe oscillations and therefore indicate that the disappearance mode, $\nu_\mu \rightarrow \nu_x$, can also be used. Accordingly, 3σ or better measurements of the hierarchy are anticipated from a variety of experiments in the coming future. Coupled with their applicability to other questions both in oscillation physics and beyond, atmospheric neutrinos will continue to enjoy an important role in measurements at both current and future experiments.

Acknowledgments

We gratefully acknowledge members of the Super-Kamiokande collaboration for useful discussions during the preparation of this manuscript. This work has been supported in part by funding from the Japanese Ministry of Education, Culture, Sports, Science and Technology and the Japan Society for the Promotion of Science.

References

[1] Fukuda Y *et al* (Super-Kamiokande Collaboration) 1998 *Phys. Rev. Lett.* **81** 1562–7
[2] Bandyopadhyay A *et al* (ISS Physics Working Group) 2009 *Rep. Prog. Phys.* **72** 106201
[3] King S F and Luhn C 2013 *Rep. Prog. Phys.* **76** 056201
[4] Fornengo N, Maltoni M, Tomas R and Valle J 2002 *Phys. Rev.* D **65** 013010
[5] Kostelecky A and Mewes M 2012 *Phys. Rev.*D **85** 096005
[6] An F *et al* (Daya Bay Collaboration) 2013 *Chin. Phys.*C **37** 011001
[7] Ahn J *et al* (RENO Collaboration) 2012 *Phys. Rev. Lett.* **108** 191802
[8] Abe Y *et al* (DOUBLE-CHOOZ Collaboration) 2012 *Phys. Rev. Lett.* **108** 131801
[9] Beringer J *et al* (Particle Data Group) 2012 *Phys. Rev.* D **86** 010001
[10] Abe K *et al* (T2K Collaboration) 2014 *Phys. Rev. Lett.* **112** 061802
[11] Kajita T 2004 *New J. Phys.* **6** 194
[12] Battistoni G, Ferrari A, Montaruli T and Sala P 2005 *Astropart. Phys.* **23** 526–34
[13] Honda M, Kajita T, Kasahara K and Midorikawa S 2004 *Phys. Rev.* D **70** 043008
[14] Barr G, Gaisser T, Lipari P, Robbins S and Stanev T 2004 *Phys. Rev.* D **70** 023006
[15] Lipari P 2000 *Astropart. Phys.* **14** 171–88
[16] Gonzalez-Garcia M, Halzen F, Maltoni M and Tanaka H K 2008 *Phys. Rev. Lett.* **100** 061802
[17] Honda M, Kajita T, Kasahara K and Midorikawa S 2011 *Phys. Rev.* D **83** 123001
[18] Enberg R, Reno M H and Sarcevic I 2008 *Phys. Rev.* D **78** 043005
[19] Aartsen M *et al* (The IceCube Collaboration) 2014 *Phys. Rev.* D **89** 062007
[20] Aguilar J *et al* (ANTARES Collaboration) 2011 *Phys. Lett.* B **696** 16–22
[21] Honda M, Kajita T, Kasahara K, Midorikawa S and Sanuki T 2007 *Phys. Rev.* D **75** 043006
[22] Battistoni G, Ferrari A, Montaruli T and Sala P 2003 *Astropart. Phys.* **19** 269–90
[23] Martin A, Ryskin M and Stasto A 2003 *Acta Phys. Pol.* B **34** 3273–304
[24] Gaisser T K 1990 *Cosmic Rays and Particle Physics* (Cambridge: Cambrige University Press)
[25] Reines F *et al* 1965 *Phys. Rev. Lett.* **15** 429–33
[26] Achar C *et al* 1965 *Phys. Rev. Lett.* **18** 196
[27] Abe K *et al* (Super-Kamiokande Collaboration) 2013 *Phys. Rev. Lett.* **110** 181802
[28] Agafonova N *et al* (OPERA Collaboration) 2013 *J. High Energy Phys.* JHEP11(2013)036
[29] Pontecorvo B 1968 *Sov. Phys—JETP* **26** 984–8
[30] Maki Z, Nakagawa M and Sakata S 1962 *Prog. Theor. Phys.* **28** 870
[31] Mohapatra R *et al* 2007 *Rep. Prog. Phys.* **70** 1757–867
[32] Albright C H and Chen M C 2006 *Phys. Rev.* D **74** 113006
[33] de Gouvea A *et al* (Intensity Frontier Neutrino Working Group) 2013
[34] Parke S 2013 *Phys. Scr.* **T158** 014013
[35] Lipari P 2004 *Proc. 5th RCCN Int. Workshop on Sub-dominant Oscillation Effects in Atmospheric Neutrino Experiments* pp 229–46
[36] Barger V, Whisnant K, Pakvasa S and Phillips R J N 1980 *Phys. Rev.* D **22** 2718
[37] Dziewonski A M and Anderson D L 1981 *Phys. Earth, Planet, Inter.* **25** 297
[38] Mikheev S and Smirnov A Y 1985 *Sov. J. Nucl. Phys.* **42** 913–7
[39] Wolfenstein L 1978 *Phys. Rev.* D **17** 2369–74
[40] Akhmedov E K 1988 *Sov. J. Nucl. Phys.* **47** 301–2
[41] Krastev P and Smirnov A Y 1989 *Phys. Lett.* B **226** 341–6
[42] Fukuda Y *et al* (Super-Kamiokande Collaboration) 2003 *Nucl. Instrum. Methods* A **501** 418–62
[43] Ashie Y *et al* (Super-Kamiokande Collaboration) 2005 *Phys. Rev.* D **71** 112005
[44] Himmel A (Super-Kamiokande) 2014 *AIP Conf. Proc.* **1604** 345–52
[45] Wendell R (Super-Kamiokande Collaboration) 2013 *Nucl. Phys.* B **237-238** 163–5
[46] Abe K *et al* (T2K Collaboration) 2013 *Phys. Rev. Lett.* **111** 211803
[47] Adamson P *et al* (MINOS Collaboration) 2013 *Phys. Rev. Lett.* **110** 251801

[48] Fukuda S *et al* (Super-Kamiokande Collaboration) 2000 *Phys. Rev. Lett.* **85** 3999–4003
[49] Mitsuka G *et al* (Super-Kamiokande Collaboration) 2011 *Phys. Rev.* D **84** 113008
[50] Abe K *et al* (Super-Kamiokande Collaboration) 2011 *Phys. Rev. Lett.* **107** 241801
[51] Davidson S, Pena-Garay C, Rius N and Santamaria A 2003 *J. High Energy Phys.* 011–JHEP03(2003)011
[52] Fechner M *et al* (Super-Kamiokande Collaboration) 2009 *Phys. Rev.* D **79** 112010
[53] Ashie Y *et al* (Super-Kamiokande Collaboration) 2004 *Phys. Rev. Lett.* **93** 101801
[54] Michael D *et al* (MINOS Collaboration) 2008 *Nucl. Instrum. Methods* A **596** 190–228
[55] Adamson P *et al* (MINOS Collaboration) 2012 *Phys. Rev.* D **86** 052007
[56] Blake A, Chapman J and Thomson M 2013 *Nucl. Instrum. Methods* A **707** 127–34
[57] Boger J *et al* (SNO Collaboration) 2000 *Nucl. Instrum. Methods* A. **449** 172–207
[58] Aharmim B *et al* (SNO Collaboration) 2009 *Phys. Rev.* D **80** 012001
[59] Karle A (IceCube Collaboration) 2010 arXiv:1003.5715
[60] Abbasi R *et al* (IceCube Collaboration) 2012 *Astropart. Phys.* **35** 615–24
[61] Aartsen M *et al* (IceCube Collaboration) 2013 *Phys. Rev. Lett.* **111** 081801
[62] Abbasi R *et al* (IceCube Collaboration) 2011 *Phys. Rev.* D **83** 012001
[63] Aartsen M *et al* (IceCube Collaboration) 2013 *Phys. Rev. Lett.* **110** 151105
[64] Kostelecky V A and Mewes M 2004 *Phys. Rev.* D **70** 076002
[65] Abbasi R *et al* (IceCube Collaboration) 2010 *Phys. Rev.* D **82** 112003
[66] Ageron M *et al* (ANTARES Collaboration) 2011 *Nucl. Instrum. Methods* A **656** 11–38
[67] Adrian-Martinez S *et al* (ANTARES collaboration) 2012 *Phys. Lett.* B **714** 224–30
[68] Wendell R *et al* (Super-Kamiokande Collaboration) 2010 *Phys. Rev.* D **81** 092004
[69] (Hyper-K Working Group) 2012 *Open Meeting for the Hyper-Kamiokande Project* http://indico.ipmu.jp/indico/conferenceDisplay.py?ovw=True&confId=7
[70] Adams C *et al* (LBNE Collaboration) 2013 arXiv:1307.7335
[71] Thakore T, Ghosh A, Choubey S and Dighe A 2013 *J. High Energy Phys.* JHEP05(2013)058
[72] Aartsen M *et al* (IceCube-PINGU Collaboration) 2014 arXiv:1401.2046
[73] Koskinen D J 2011 *Mod. Phys. Lett.* A **26** 2899–915
[74] Akhmedov E K, Razzaque S and Smirnov A Y 2013 *J. High Energy Phys.* JHEP02(2013)082
[75] Katz U F (KM3NeT Collaboration) 2014 *PoS* arXiv:1402.1022
[76] Ge S F and Hagiwara K 2014 *J. High Energy Phys.* JHEP09(2014)024
[77] Kooijman P *et al* (KM3NeT Collaboration) 2013 *ICRC*